Dyes and Pigments 92 (2011) 580–587

Contents lists available at ScienceDirect

Dyes and Pigments

journal homepage: www.elsevier.com/locate/dyepig

Photophysical properties of arylcarbonitrile derivatives: Synthesis, absorption and emission spectra, and quantum chemical studies

Yasuhiro Shigemitsu [a,*], Bo-Cheng Wang [b], Yasuhisa Nishimura [c], Yoshinori Tominaga [c]

[a] Industrial Technology Center of Nagasaki, 2-1303-8 Ikeda, Omura, Nagasaki 856-0026, Japan
[b] Department of Chemistry, Tamkang University, Tamsui 251, Taiwan
[c] Faculty of Environmental Studies, Nagasaki University, 1-14, Bunkyo-machi, Nagasaki 852-8131, Japan

ARTICLE INFO

Article history:
Received 24 April 2011
Received in revised form
8 June 2011
Accepted 9 June 2011
Available online 22 June 2011

Keywords:
Aromatic cyanovinyl compounds
DFT
CASSCF
Electronic spectra
Fluorescence spectra
Conical Intersections

ABSTRACT

A new series of aromatic cyanovinyl compounds were synthesized via one-pot reactions of tri- or tetracyanoethylenes with nucleophilic reagents. The ground-state geometries and UV–vis absorption spectra of the compounds were computationally analyzed by means of density functional theory (DFT) and time-dependent density functional theory (TDDFT) calculations, respectively. None of the compounds were fluorescent in solution, but some showed intense emission in the solid state. The first excited singlet states (S_1) potential energy surfaces (PESs) were explored using complete active space SCF (CASSCF) calculations for the compounds in order to elucidate nonradiative decay mechanism that takes into account the involvement of conical intersections (CI).

1. Introduction

Polarized cyanoethylenes bearing intramolecular push–pull electronic structures are widely used as key synthetic reagents [1]. In the course of our work on the use of asymmetrically substituted ethylenes as synthetic building blocks, we found a series of new dyes that are fluorescent not only in solution but also in the solid state [2,3].

In the present study, we describe the UV–vis absorption and solid-state fluorescence spectra of a series of aromatic cyanovinyl compounds. Organic luminescent materials have potential for a wide range of photofunctional applications, such as nonlinear optics [4] and fluorescent biosensors [5]. In particular, the solid-state luminescence of these materials has received much attention for use in organic light-emitting diodes (OLEDs) [6]. Among the various OLED candidates, fluorescent styryl derivatives are particularly promising because of their efficient emission properties and flexibly tunable chemical structures. 4-(dicyanomethylene)-2-methyl-6-(*p*-dimethylaminostyryl)-4*H*-pyran (DCM) has been employed in red OLED materials and widely studied by means of spectroscopic techniques and quantum chemistry computations [7–9].

This study aims to synthesize a series of aromatic cyanovinyl compounds and to find an underlying link between the spectral features and the structural parameters using quantum chemistry calculations. Time-dependent density functional theory (TDDFT) calculations were employed in order to obtain qualitative accuracies in the prediction of valence excitation energies [10].

2. Methods

2.1. Syntheses

Preparations of asymmetrically substituted ethylenes are in remarkable progress. As an interesting example, sophisticated synthesis under ultrasound irradiation has been reported to obtain tricyanovinyl aromatic amines [11]. In the present study, simple one-step synthetic methods [12] were employed to obtain the series of aromatic di- and tricyanovinyl compounds. The strategy was applied for the reaction of *N*,*N*-dimethylaniline [13] and 1-methyl-1*H*-pyrrole [14] with tetracyanoethylene. The reaction of tetracyanoethylene and nucleophilic heterocycles **1**–**6** in dimethyformamide produced good yields of the corresponding aromatic tricyanovinyl compounds, **7a, 8a, 9a, 10a**, **11a,** and **12a**, as shown in

* Correspondence author. Tel.: +81 957 52 1133; fax: +81 957 52 1136.
E-mail address: shige@tc.nagasaki.go.jp (Y. Shigemitsu).

0143-7208/$ – see front matter © 2011 Elsevier Ltd. All rights reserved.
doi:10.1016/j.dyepig.2011.06.015

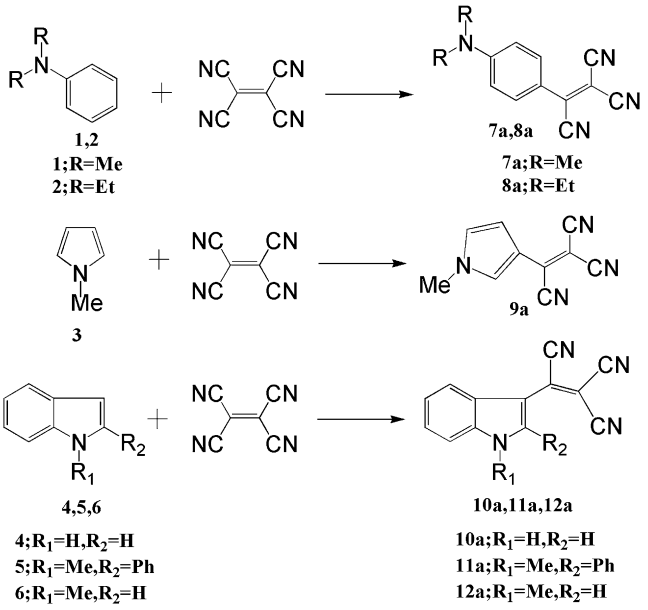

Fig. 1. Synthetic scheme of aromatic tricyanovinyl compounds **(7a, 8a, 9a, 10a, 11a, 12a)**.

Fig. 1. The aromatic dicyanovinyl compounds **7b–h**; **8b–d**; **9b,c**; **10b,c**; **11b,c**; **and 12b,c** were readily synthesized via one-pot substitution reactions of aromatic tricyanoethylene with amines, as shown in Fig. 2. The details of the syntheses are described in Experimental section.

2.2. Computational details

The ground-state (S_0) geometries were fully optimized by density functional theory (DFT) with Pople's standard basis sets 6–31G(d,p) in conjunction with the hybrid functional B3LYP. TDDFT/6–31 + G(d,p) calculations with B3LYP and two new functionals (LC-wPBE [15] and CAM-B3LYP [16]) were performed for the DFT-optimized geometries in aiming to evaluate the vertical excitation energies. Solvent effects for ethanol were considered with the conventional linear-response Polarized Continuum Model (PCM) [17] for the DFT and TDDFT calculations. Semi-empirical ZINDO spectral calculations were also carried out with the preset parameters. The strategies employed here were quantitatively verified in our previous report [18]. The torsional scan of S_1 states were performed at the points with all other geometrical parameters being fully optimized, using CI-singles (CIS/6–31G(d,p)) and 4 state-average CASSCF with 6 active electrons distributed in 6 active π-orbitals using atomic natural orbital (3s2p1d/2s1p:DZP) basis set (SA4-CASSCF(6,6)/ANO-S), respectively. The choice of active space was done according to the orbital occupation numbers larger than 0.095, including the electron redistribution configurations from amine to cyanoethylene moiety. The active space excluded *n*-orbitals because they lie considerably below the HOMOs and give negligibly small contributions to the S_1 states. S_0/S_1-Conical intersections were located with CASSCF(10,10)/ANO-S-MB (minimal base) level, where the enlarged active space was necessary to obtain smooth geometry convergence. DFT, TDDFT, and ZINDO calculations were done with Gaussian09 software [19]. CASSCF calculations were performed with MOCAS ver.7.4 software [20].

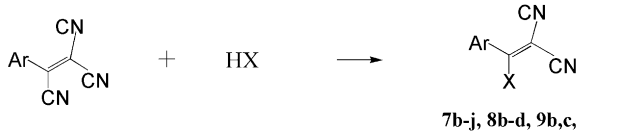

Entry	Ar	X
7b	1	NH_2
7c	1	$N(CH_3)_2$
7d	1	$NH(CH_3)$
7e	1	$(CH_2)_4N$
7f	1	$(CH_2)_5N$
7g	1	$N(CH_2)_4O$
7h	1	$N(CH_2)_4S$
7i (*)	1	H
7j (*)	1	SMe

Entry	Ar	X
8b	2	$N(CH_3)_2$
8c	2	$NH(CH_3)$
8d	2	$N(CH_2)_4O$
9b	3	$N(CH_3)_2$
9c	3	$N(CH_2)_4O$
10b	4	$N(CH_3)_2$
10c	4	$N(CH_2)_4O$
11b	5	$N(CH_3)_2$
11c	5	$N(CH_2)_4O$
12b	6	$N(CH_3)_2$
12c	6	$N(CH_2)_4O$

Fig. 2. Synthetic scheme of aromatic dicyanovinyl compounds **(7b–7j, 8b–8d, 9b–c, 10b–c, 11b–c, 12b–c)**.

3. Results and discussion

3.1. Absorption spectra

The UV–vis spectra of the aromatic cyanovinyl compounds measured in ethanol at room temperature exhibited intense π–π* peaks in the visible region, accompanied by minor peaks in the region below 300 nm. The aromatic tricyanovinyl compounds showed λ_{max} at approximately 500 nm, with the exception of **9a** which bears a methylpyrrole ring and showed a maximum at 389 nm. **8a** bearing a diethylaminophenyl group showed the most bathochromic shift with the peak at 526 nm. The λ_{max} of the aromatic tricyanovinyl compounds were considerably red-shifted relative to those of the aromatic dicyanovinyl compounds, with the exception of **7e**, which showed the peak at 302 nm. The hypsochromic λ_{max} shifts of the aromatic dicyanovinyl compounds (except for **7i** and **7j**) relative to the those of the aromatic tricyanovinyl compounds are presumably derived from a weakening of the intramolecular push–pull electronic structures due to the substitution of one of the cyano groups by a nitrogen-containing electron-donating group.

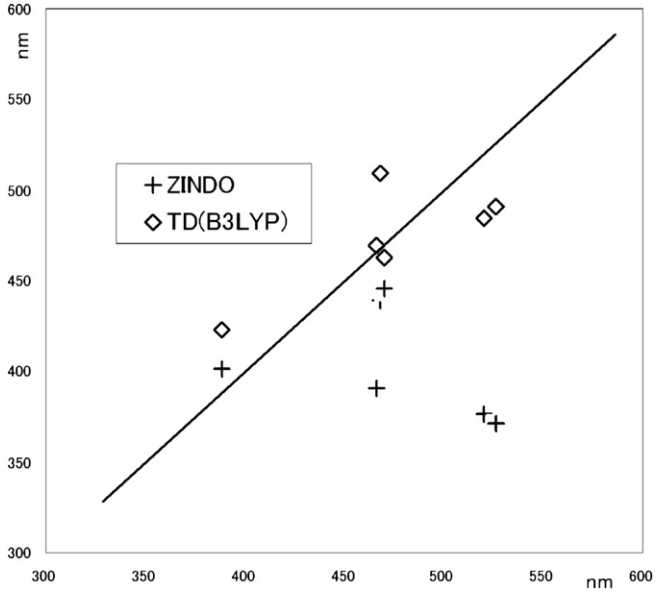

Fig. 3. Correlation between experimental and theoretical λ_{max} for aromatic tricyanovinyl compounds.

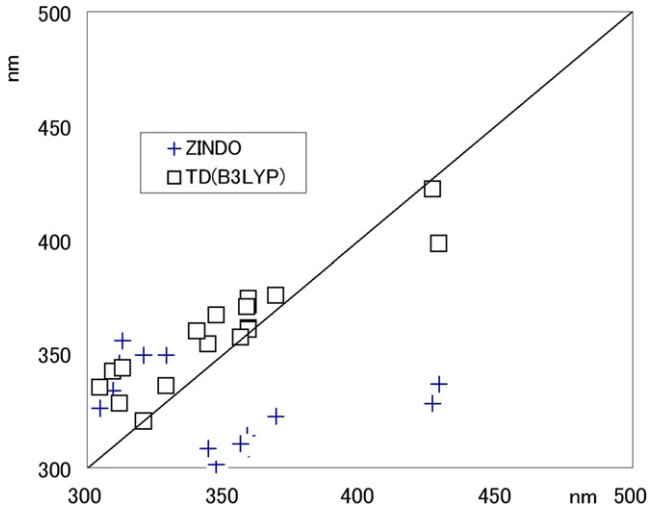

Fig. 4. Correlation between experimental and theoretical λ_{max} for aromatic dicyanovinyl compounds.

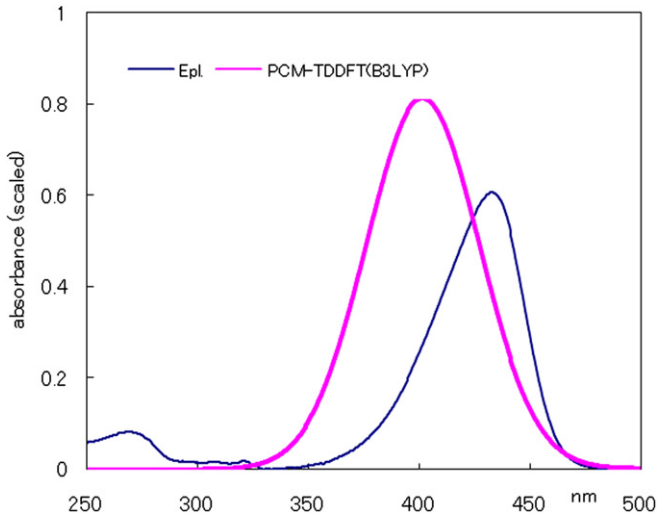

Fig. 6. The experimental and simulated absorption spectrum of **7j**. Gaussian broadning with half-bandwidth $\Delta_{1/2} = 5000\ cm^{-1}$ for the simulated spectrum.

The correlations between the experimental and computational λ_{max} are presented in Fig. 3 for the aromatic tricyanovinyl compounds, and 4 for the aromatic dicyanovinyl compounds, respectively. ZINDO and TDDFT computations consistently assigned the first intense peaks λ_{max} to the $\pi-\pi^*$ HOMO–LUMO excitations with large oscillator strengths. The HOMOs have a bonding character on the ethylene unit and lobes on the amine moiety, while the LUMOs have an anti-bonding character on the ethylene unit and lobes on the cyano groups. The S_0->S_1 excitations, therefore, invoke intramolecular electron transfer from the electron-donating moiety (amine) to the electron withdrawing moiety (cyanoethylene). The calculated λ_{max} predicted by ZINDO tended to be at shorter wavelengths than the experimental λ_{max}. The ZINDO method is known to systematically overestimate the experimental vertical excitation energies as the π-conjugation length elongates, owing to the imbalance between the one- and two-electron parts of the electronic transition energy [21]. The correlations between the experimental and computational λ_{max} are presented in Fig. 3 for the aromatic tricyanovinyl compounds, and Fig. 4 for the aromatic dicyanovinyl compounds, respectively.

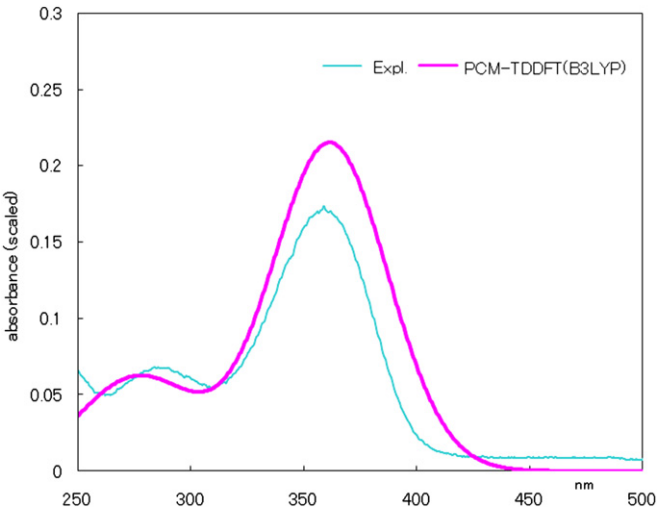

Fig. 5. The experimental and simulated absorption spectrum of **7b**. Gaussian broadning with half-bandwidth $\Delta_{1/2} = 5000\ cm^{-1}$ for the simulated spectrum.

The experimental and TDDFT(B3LYP)-predicted absorption spectra for **7b** and **7i** are superimposed in Figs. 5 and 6, respectively. The TDDFT(B3LYP)-predicted spectra were created by applying uniform Gaussian broadening and were adequately scaled for comparison with the experimental spectra. For **7b**, the peak position, peak intensity, and overall shape were reproduced well by the TDDFT(B3LYP) simulation. For **7i**, however, the shape was not reproduced quantitatively. The second peak with a smaller oscillator strength was missing from the 250–300-nm region. This failure is presumably due to inherent limitations of the B3LYP [22].

To improve TDDFT(B3LYP) prediction accuracies, we applied two new functionals, LC-wPBE and CAM-B3LYP, to the compounds. These functionals were designed to correct the inaccurate

Table 1
Computed absorption maxima of **(8, 9, 10, 11, 12)** using three exchange-correlation functional (LC-wPBE, CAM-B3LYP, B3LYP) along with experimental maxima.

Entry	Abs max (nm)			
	LC-wPBE	CAM-B3LYP	B3LYP	expl.
7a	414	443	484	520
7b	299	321	361	359
7c	296	319	367	348
7d	290	312	355	345
7e	281	306	360	302
7f	288	311	361	359
7g	300	306	371	359
7h	300	332	374	359
7i	355	372	398	429
7j	349	374	422	427
8a	416	446	491	526
8b	298	321	371	359
8c	291	311	357	356
8d	302	326	376	369
9a	356	380	423	389
9b	278	290	328	312
9c	279	291	320	321
10a	384	412	469	453
10b	282	299	335	305
10c	282	300	342	310
11a	404	446	516	468
11b	286	306	346	291
11c	286	311	356	293
12a	393	306	563	470
12b	287	308	356	329
12c	288	308	363	313

Table 2
Fluorescence spectra of **(8, 9, 10, 11, 12)** in solid state.

Entry	Em max (nm)	SS	RI
7a	484	119	0.02
7b	460	139	5.40
7c	445	107	0.75
7d	441	93	1.43
7e	431	86	0.59
7f	436	90	2.79
7g	445	111	2.78
7h	442	124	1.65
7i	561	229	0.09
7j	539	196	0.09
8a	449	98	0.03
8b	435	90	1.56
8c	436	105	2.94
8d	461	106	1.64
9a	526	188	0.33
9b	495	145	0.06
9c	438	89	1.12
10a	578	238	0.05
10b	441	92	0.86
10c	445	81	0.06
11a	447	101	0.04
11b	445	103	0.08
11c	441	93	2.01
12a	593	248	0.00
12b	457	101	0.00
12c	430	81	0.00

SS: Stokes Shift.
RI: Relative fluorescece intensity.

asymptotic behavior of the Coulomb potential in the long-range region. The calculated λ_{max}, however, were not improved than those obtained using B3LYP (Table 1). LC-wPBE overestimated the S_0–S_1 transition energies, with deviations of approximately 100 nm. CAM-B3LYP showed better agreements than LC-wPBE, but neither functional outperformed the popular B3LYP for the compounds. Significant overestimations by LC-wPBE and CAM-B3LYP have also been reported for medium-sized molecules, such as substituted anthraquinones [23] and malononitrile derivatives [24].

3.2. Fluorescence spectra and excited state dynamics

The solid-state fluorescence spectra of the compounds consistently showed an unstructured single band with a maximum in the range from 430 nm (**12c**) to 593 nm (**12a**) as shown in Table 2. The relative fluorescence intensities (RIs) were measured using tris(8-hydroxyquinolinato)aluminium as a standard. All the aromatic tricyanovinyl compounds showed very small RIs, whereas some of aromatic dicyanovinyl compounds had large RIs: **7b** (5.40), **7f** (2.79), **7g** (2.78), **8c** (2.94), and **11c** (2.01). The switch in the electronic nature of the ethylene unit due to the change from an inert

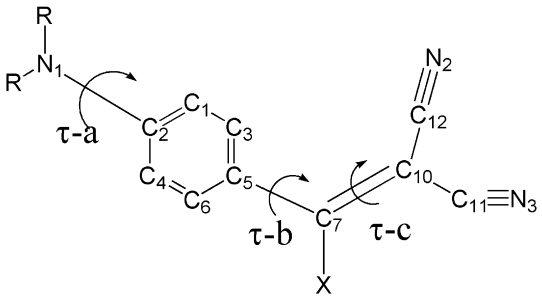

Fig. 7. Key twist angle definitions (τ-a, τ-b, τ-c) of the aromatic cyanovinyls.

Table 3
Computed bond lengths and twist angles in S_0 and S_1 state of **(7b, 7i)**.

Parameter	S_0-min		S_1-min	
	DFT	CAS	CIS	CAS
7b				
N_1–C_2	1.358	1.389	1.384	1.393
C_5–C_7	1.469	1.475	1.453	1.430
C_7–C_{10}	1.396	1.372	1.424	1.471
C_{10}–C_{11}	1.423	1.439	1.433	1.427
C_{11}–N_3	1.117	1.137	1.140	1.139
τ-a	2.98	15.2	13.5	17.0
τ-b	33.6	41.7	18.1	10.9
τ-C	8.57	7.27	89.9	88.7
7i				
N_1–C_2	1.371	1.370	1.366	1.326
C_5–C_7	1.438	1.453	1.432	1.379
C_7–C_{10}	1.374	1.337	1.421	1.454
C_{10}–C_{11}	1.432	1.446	1.431	1.399
C_{11}–N_3	1.164	1.137	1.140	1.151
τ-a	0.01	0.05	0.09	0.10
τ-b	0.02	0.10	0.00	0.00
τ-C	0.01	0.06	90.0	90.0

substituent (H) to heterocyclic units can be expected to alter the emission properties. By contrast, emission spectra were absent or very weak in the solution state for all the compounds.

In the relaxation of excited states, several nonradiative processes are involved in the modulation of the emissive properties, including intersystem crossing to triplet states, intra- and intermolecular vibrational relaxation, and ultrafast conversion from the nonemissive Franck–Condon state to the emissive TICT state [25].

Swalina et al. computationally investigated **7i** (4-*N*,*N*-dimethylaminobenzylidenemalononitrile) for the S_1 potential energy surface (PES) using several *ab initio* methods [26]. They used a two state-average CASSCF method to explore the S_0 and S_1 PES on the S_0-optimized geometry. The result showed that, of the three key rotational freedoms of the molecules (τ-a, τ-b, τ-c shown in Fig. 7), the twisting motion around the ethylene unit (τ-c), is most important in governing the fluorescence properties in the S_1 state. The CASSCF computations successfully located the S_0/S_1-CI which is perpendicularly distorted around τ-c. The satisfactory result is, however, limited within the qualitative accuracy because the geometries were optimized for the S_0 state, not the S_1 state.

We herein carried out S_0-geometry optimizations using DFT and CASSCF, and S_1-geometry optimizations using CIS and CASSCF, in vacuo and in solution, for **7b** and **7i**. The two aromatic dicyanovinyl

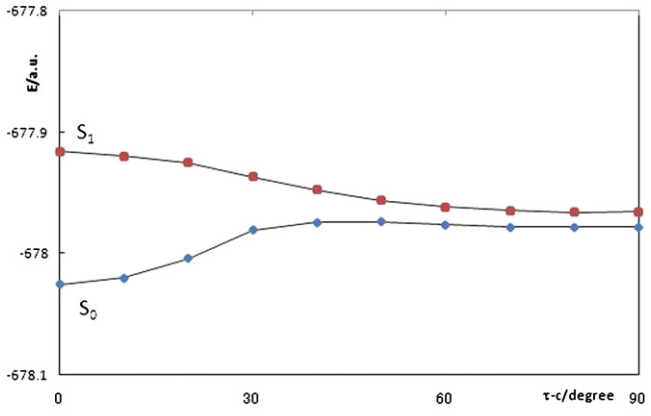

Fig. 8. S_0 and S_1 PES of **7b** with variation of the twist angle τ-c.

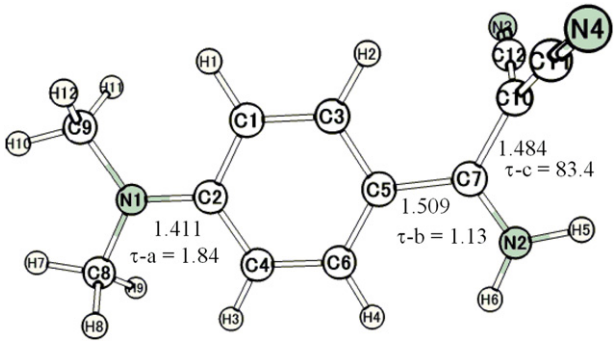

Fig. 9. Opimized geometry at S_0/S_1-MECI for **7b**.

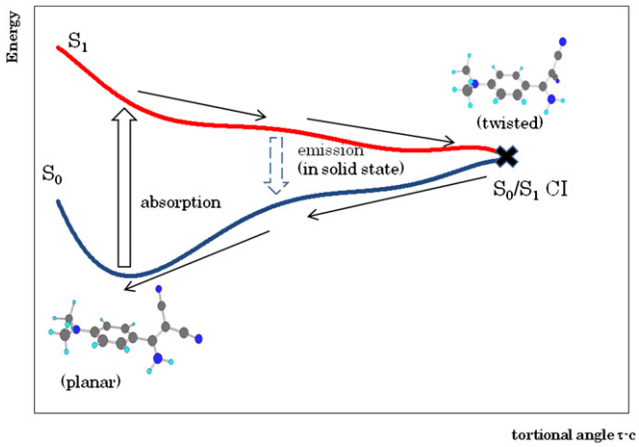

Fig. 11. Schematic diagram of S_1 state dynamics of **7b**.

compounds were focused on because they exhibit drastic differences in the fluorescence intensities in solid state; **7b** (intense) and **7i** (weak).

DFT-level geometry optimization for the S_0 state showed that the dimethylaminophenyl ring of **7b** was distorted around τ-b by 33.6° because of the steric repulsion between the ring and the amino group, whereas **7i** held an in-plane orientation due to the absence of intramolecular steric crowding. CIS-level geometry optimization for the S_1 state found an almost perpendicular distortion form around the central ethylene unit both for **7b** and **7i**. Interestingly, **7i** retained a flat geometry with inclusion of solvent effect (PCM = ethanol).

For **7b**, CASSCF geometry optimizations for S_1 along τ-c variation showed that the most stable form was a nearly planar structure for S_0 and an almost perpendicular structure for S_1, respectively (Table 3 and Fig. 8). The results are consistent with those determined at CIS level abovementioned. The τ-b varied more considerably in the S_0 state than in the S_1 state. A S_0/S_1-CI was found at a perpendicularly distorted form which is located at 1.9 kcal/mol above the S_1 energy-minimized point at τ-c = 90°. A minimum-energy S_0/S_1-CI (MECI) with a twist angle of 83.4° was located at 0.4 kcal/mol lower than the S_0/S_1-CI at 90°. The optimized geometry of S_0/S_1-MECI was shown in Fig. 9.

For **7i**, CASSCF geometry optimizations for S_1 along τ-c variation produced the qualitatively similar PES to that for **7b** (Fig. 10). The S_0 and S_1 PES obtained here are consistent with those obtained by Swalina et al. [21], which were computed on the S_0-optimized geometries. Both S_1 PESs monotonically decrease in energy and possess no barrier for τ-c variation. A S_0/S_1-CI was found at a perpendicularly distorted form which is located at 10.6 kcal/mol above the S_1 energy-minimized point at τ-c = 90°. The S_0–S_1 gap obtained here sharply narrows over the range τ-c being less than

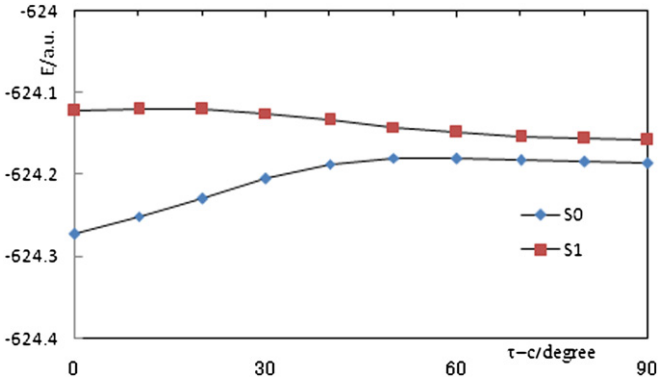

Fig. 10. S_0 and S_1 PES of **7i** with variation of the twist angle τ-c.

40° and the presence of S_0/S_1 energy crossing seam is indicated over the range τ-c being more than 60°. Meanwhile, the gap computed by Swalina et al. [26] remains insensitive up to τ-c = 30° and then sharply decreases toward a S_0/S_1-CI at τ-c = 90°. The quantitative inconsistencies between the two results are presumably derived from the differences in geometry optimization states (for S_0 or S_1) and CASSCF methodologies (active space and basis sets). Furthermore, dynamical correlation defect in CASSCF computations can alter the PES landscape quantitatively.

The common PES landscape for **7b** and **7i** in the S_0 and S_1 states explains that the two molecules exhibit no emission in solution because the nonradiative deactivation pathways through the S_0/S_1-CI work efficiently (Fig. 11).

The larger compounds (**9**–**12**) generally showed a weaker fluorescence in the solid state than (**7**–**8**), with the exceptions of **9c** and **11c**, which have a morpholine group. Nonemissive energy dissipation pathways are enhanced in larger molecules through the greater number of vibration freedoms. The bulky morpholine group of **9c** and **11c** can disrupt the twisting motion of cyano group, leading these compounds to remain fluorescent in the solid state.

In conclusion, S_0/S_1-CIs found in the present study strongly suggest a presence of efficient nonradiative relaxation path from S_1 to S_0. The modest fluorescence for the several molecules in the solid state indicates the critical role of CIs, which can act as efficient deactivation paths in solution but become deactivated by steric hindrance in the solid state. Alternatively, molecular twisting in the S_1 state can lower the fluorescence quantum yield because the displacement of the S_1 PES relative to the ground-state PES induces a larger overlap with the vibration levels in the ground state, thereby opening efficient nonradiative decay channels [27].

4. Conclusions

We synthesized a series of aromatic cyanovinyl compounds via the reaction of tri- or tetracyanoethylenes with nucleophiles. Quantum chemical analysis of the absorption spectra verified the considerable red shifts of the absorption maxima of the aromatic dicyanovinyl compounds relative to that of the aromatic tricyanovinyl compounds. The spectral shapes of **7b** and **7i** calculated by TDDFT(B3LYP) were qualitatively coincident with the experimental shapes. Two new functionals (LC-wPBE and CAM-B3LYP) did not outperform B3LYP in that the two functionals significantly overestimated the S_0–S_1 transition energies. A state-specific PCM [28] including dynamical solvent effects can considerably improve the predictions of the two functionals, because nonequilibrium solvent

polarization can be adequately treated by the new PCM particularly for such intramolecularly push–pull systems as in this study.

All the compounds showed no or negligible fluorescence in solution, but some of the aromatic dicyanovinyl compounds exhibited intense fluorescence in the solid state. The CASSCF calculations in vacuo revealed that **7b** and **7i** were stabilized in the S_1 state by the twisting motion around the ethylene unit. The nearly perpendicular forms in the S_1 state reached the S_0/S_1-CI and swiftly go back to the S_0 state nonradiatively. The drastic differences in fluorescence intensity between **7b** (strongly emissive) and **7i** (nonemissive) in the solid state were explained by the different magnitude of intermolecular steric hinderance that made the CIs inaccessible only for **7b**.

5. Experimental section

All melting points were determined in a capillary tube and are uncollected. The Infrared (ir) spectra were recorded in potassium bromide pellets using a JASCO 810 spectrometer and ultraviolet (uv) absorption spectra were determined in 95% ethanol using a Shimadzu UV3100pc spectrometer. Fluorescence spectra were determined on a Shimadzu RF-5300pc spectrofluorometer. Nuclear magnetic resonance (nmr) spectra were obtained using Gemini 300NMR(300 MHz) and JEOL-GX-400(400 MHz) spectrometers with tetramethylsilane as the internal standard. Mass(ms) spectra were recorded on JEOL MS-DX303 mass spectrometer. Elemental analyses were performed at the Microanalytical Laboratory of the Center for Instrumental Analysis in Nagasaki University.

5.1. 1-(4-Dimethylaminophenyl)ethene-1,2,2-tricarbonitrile (7a)

A solution of 0.605 g of *N,N*-dimethylaniline and 0.640 g of tetracyaniethylene in 20 ml of DMF was heated for 30 min at 50–60 °C. After cooling, the precipitate that appeared was collected by filtration and recrystallized from methanol to give 1.054 g (95% yield) of purple needles, mp 173–175 °C. IR(KBr) ν_{max} cm^{-1}: 2212(CN), 1607, 1492. UV(ethanol)λ_{max} nm(log ε): 256(3.37), 294(3.28), 520(3.82). ^{1}H-NMR($CDCl_3$)δ: 3.22(6H, s, NMe_2), 6.75(2H, d, J = 9.4 Hz, 3,′-H), 8.08(2H, d, J = 9.4 Hz, 2,6-H).

5.2. 2-[Amino-(4-dimethylaminophenyl)methylene]malononitrile (7b)

A solution of 0.22 g of **7a** in 100 ml of aqueous ammonia was refluxed for 40 min. After cooling, the precipitate that appeared was collected by filtration and recrystallized from methanol to give 0.133 g (63% yield) of white needles, mp 235–238 °C. IR(KBr) ν_{max} cm^{-1}: 3365(NH), 3227(NH), 2214(CN), 2197(CN), 1658, 1601, 1509, 1434, 1207. UV(ethanol)λ_{max} nm(log ε): 359(4.24), 284(3.83). ^{1}H-NMR($CDCl_3$)δ: 1.99(2H,s,–NH2), 3.41(6H,s,NMe), 6.73(1H,s,NH), 7.14(1H,s,NH).

5.3. 2-[Dimethylamino-(4-dimethylaminophenyl)methylene] malononitrile (7c)

A mixture of 0.888 g of **7a** with 0.300 g of dimethylamine was heated for 5 min at 200 °C when the reddish crystals completely disappeared. After cooling, the precipitate washed with water was collected by filtration and recrystallized from methanol to give 0.736 g (77% yield) of yellow needles, mp 130–135 °C. IR(KBr) ν_{max} cm^{-1}: 2901, 2200(CN), 2184(CN), 1604, 1561, 1421, 1190. UV(ethanol)λ_{max} nm(log ε): 564(1.69), 349(5.28), 226(5.02). ^{1}H-NMR($CDCl_3$)δ: 3.05(12H,s,NMe), 6.69(2H,d,J = 8.9,3,5-H), 7.26(2H,d,J = 8.9,2,6-H).

5.4. 2-[(4-Dimethylaminophenyl)(methylamino)methylene] malononitrile (7d)

This compound was obtained from 0.466 g of **7a** mixed with 0.100 g of methylamine in a similar manner to that of **7c**, giving 0.417 g (88% yield) of yellow needles. IR(KBr) ν_{max} cm^{-1}: 3287(NH), 2917, 2209(CN), 2195(CN), 1605, 1410, 1173. UV(ethanol)λ_{max} nm(log ε): 344(4.11), 295(4.01). ^{1}H-NMR($CDCl_3$)δ: 2.98(3H,s,NMe), 3.05(6H,s,NMe), 6.12(1H,s,NMe), 6.72(2H,d,J = 8.1,3,5-H), 7.30(2H,d,J = 8.8,2,6-H).

5.5. 2-[(4-Dimethylaminophenyl)pyrrolidin-1-yl-methylene] malononitrile (7e)

This compound was obtained from 0.222 g of **7a** mixed with 0.100 g of pyrrolidine in a similar manner to that of **7c**, giving 0.177 g (67% yield) of white needles, mp 128–129 °C. IR(KBr) ν_{max} cm^{-1}: 2976, 2881, 2808, 2198(CN), 2182(CN), 1607, 1520, 1421, 1210. UV(ethanol)λ_{max} nm(log ε): 302(4.38), 226(4.71). ^{1}H-NMR($CDCl_3$)δ: 1.84(1H,w,–CH2–), 2.09(2H,w,–CH2–), 3.34(2H,w,N–CH2), 3.97(2H,w,N–CH2), 6.68(2H,d,J = 9.0,3-5H), 7.17(2H,d,J = 9.0,2,6-H).

5.6. 2-[(4-Dimethylaminophenyl)piperidin-1-yl-methylene] malononitrile (7f)

This compound was obtained from 0.222 g of **7a** mixed with 0.120 g of piperidine in a similar manner to that of **7c**, giving 0.198 g (71% yield) of white needles, mp 145–150 °C. IR(KBr) ν_{max} cm^{-1}: 2946, 2859, 2205(CN), 2192(CN), 1603, 1523, 1426, 1208. UV(ethanol)λ_{max} nm(log ε): 359(3.91). ^{1}H-NMR($CDCl_3$)δ: 1.73(6H,s,–CH2–), 2.98(4H,s,NCH2–), 3.05(6H,s,NMe), 6.68(2H,d,J = 8.9,3–5H), 7.28(2H,d,J = 8.9,2,6-H).

5.7. 2-[(4-Dimethylaminophenyl)(morpholino)methylene] malononitrile (7g)

This compound was obtained from 0.222 g of **7a** mixed with 0.120 g of morpholine in a similar manner to that of **7c**, giving 0.153 g (68% yield) of yellow grains, mp 252–256 °C. IR(KBr) ν_{max} cm^{-1}: 3007, 2964, 2901, 2854, 2210(CN), 2194(CN), 1602, 1503, 1431, 1201. UV(ethanol)λ_{max} nm(log ε): 359(4.49), 285(3.99), 226(4.67). ^{1}H-NMR($CDCl_3$)δ: 3.06(6H,s,NMe), 3.51–3.89(8H,bs,–CH2–), 6.90(2H,d,J = 8.9,3–5H),7.30(2H,d,J = 8.9,2,6-H).

5.8. 2-[(4-Dimethylaminophenyl)(thiomorpholino)methylene] malononitrile (7h)

This compound was obtained from 0.660 g of **7a** mixed with 0.461 g of thiomorpholine in a similar manner to that of **7c**, giving 0.589 g (66% yield) of yellow grains, mp 178–180 °C. IR(KBr) ν_{max} cm^{-1}: 2907, 2207(CN), 2193(CN), 1601, 1517, 1430, 1212. UV(ethanol)λ_{max} nm(log ε): 359(4.05), 336(3.76), 316(3.23). ^{1}H-NMR($CDCl_3$)δ: 2.77(4H,bs,S–CH2–), 3.06(6H,s,NMe), 3.87(4H,bs,N–CH2–), 6.69(2H,d,J = 8.9,3-5H), 7.28(2H,d,J = 8.9,2,6-H).

5.9. 2-[(4-Dimethylaminophenyl)]malononitrile (7i)

This compound was synthesized via the scheme in reference [8]. Mp 173–175 °C. IR(KBr) ν_{max} cm^{-1}: 2210(CN), 1615, 1560, 1521. UV(ethanol)λ_{max} nm(log ε): 429(3.88).

5.10. 2-[(4-Dimethylaminophenyl)(methylsulfanyl)methylene] malononitrile (7j)

This compound was synthesized via the scheme in reference [8]. Mp 97 °C. IR(KBr) ν_{max} cm^{-1}: 2211(CN), 2190(CN), 1604, 1475. UV(ethanol)λ_{max} nm(log ε): 427(4.29), 322(3.94).

5.11. 1-(4-Diethylaminophenyl)ethene-1,2,2-tricarbonitrile (8a)

This compound was obtained from 0.298 g of *N,N*-diethylaniline mixed with 0.256 g of tetracyanoethylene in a similar manner to that of **7a**, giving 0.425 g (85% yield) of purple needles. Mp 133–135 °C. IR(KBr) ν_{max} cm^{-1}: 3275, 2979, 2212(CN), 1604, 1490, 1457, 1424. UV(ethanol)λ_{max} nm(log ε): 526(4.63), 289(3.92), 258(3.93).

5.12. 2-{Diethylamino[(4-diethylaminophenyl)methylene]} malononitrile (8b)

This compound was obtained from 0.250 g of **8a** mixed with 0.100 g of dimethylamine in a similar manner to that of **7c**, giving 0.106 g (85% yield) of white needles. Mp 119–121 °C. IR(KBr) ν_{max} cm^{-1}: 2971, 2203(CN), 2198(CN), 1603, 1519, 1437, 1195. UV(ethanol)λ_{max} nm(log ε): 477(2.23), 358(4.24). ^{1}H-NMR($CDCl_3$)δ: 1.20(5H,t,J = 7.1 Hz, −CH2−CH3), 1.53(6H,s,NMe), 3.39(5H,q,J = 7.1 Hz, −CH2−CH3), 6.64(2H,d,J = 9.1 Hz, 3,5-H), 7.22(2H,d,J = 9.1 Hz, 2,6-H).

5.13. 2-[(4-Diethylaminophenyl)(morpholino)methylene] malononitrile (8c)

This compound was obtained from 0.125 g of **8a** mixed with 0.100 g of morpholine in a similar manner to that of **7c**, giving 0.123 g (80% yield) of yellow needles. Mp 172–174 °C. IR(KBr) ν_{max} cm^{-1}: 2969, 2912, 2856, 2201(CN), 2124(CN), 1603, 1509, 1198. UV(ethanol)λ_{max} nm(log ε): 369(4.36), 320(4.15), 224(4.31). ^{1}H-NMR($CDCl_3$)δ: 1.20(5H,t,J = 7.1 Hz, −CH2−CH3), 3.40(5H,q,J = 7.1 Hz, −CH2−CH3), 3.60–3.84(8H,brs,N−CH2−), 6.65(2H,d,J = 9.1 Hz, 3,5-H), 7.27(2H,d,J = 9.1 Hz, 2,6-H).

5.14. 1-(1-Methyl-1H-pyrrol-2-yl)ethene-1,2,2-tricarbonitrile (9a)

A solution of 0.243 g of 1-methyl-1H-pyrrole and 0.384 g of tetracyaniethylene in 20 ml of DMF was heated for 15 min at 50–60 °C. After cooling, the precipitate was washed with water and was collected by filtration and recrystallized from methanol to give 0.394 g (72% yield) of yellow grains, mp 180–184 °C. IR(KBr) ν_{max} cm^{-1}: 3114, 2217(CN), 1539. UV(ethanol)λ_{max} nm(log ε): 389(4.28), 225(4.22).

5.15. 2-{Dimethylamino[(1-methylpyrrol-2-yl)methylene]} malononitrile (9b)

This compound was obtained from 0.091 g of **9a** mixed with 0.050 g of dimethylamine in a similar manner to that of **7c**, giving 0.098 g (82% yield) of transparent needles. Mp 114–116 °C. UV(ethanol)λ_{max} nm(log ε): 312(4.12), 225(4.21).

5.16. 2-[(1-Methylpyrrol-2-yl)(morpholino)methylene] malononitrile (9c)

This compound was obtained from 0.277 g of **9a** mixed with 0.150 g of morpholine in a similar manner to that of **7c**, giving 0.243 g (67% yield) of transparent needles. Mp 154–158 °C. IR(KBr) ν_{max} cm^{-1}: 3119, 2979, 2933, 2859, 2197(CN), 2080(CN), 1524, 1445, 1206. UV(ethanol)λ_{max} nm(log ε): 342(3.19), 335(3.21), 320(3.24), 226(4.10). 1H-NMR($CDCl_3$)δ: 3.70–3.82(8H,brs,N−CH2−), 3.71(3H,s,NMe), 6.17(1H,dd,J = 2.7 Hz, 1.8 Hz, 4-H), 6.67(1H,dd,2.7 Hz, 0.9 Hz, 3-H), 7.15(1H,dd,0.9 Hz, 1.8 Hz, 5-H).

5.17. 2,3-Dicyano-3-(3-indolyl) acrylonitrile (10a)

This compound was synthesized via the scheme in reference [8]. Mp:206–207 °C. IR(KBr) ν_{max} cm^{-1}:3262, 2223(CN), 1481, 1420, 1231, 1211, 1125. UV(ethanol)λ_{max} nm(log ε): 249(3.73), 284 nm(3.78), 355 nm(3.98), 466 nm(4.21).

5.18. 2-Cyano-3-(3-indolyl)-3-dimethylamino acrylonitrile (10b)

A solution of 0.218 g of **10a** and 1.0 g of dimethylamine (excessive volume) was gradually heated for 5 min. After cooling, the precipitate was washed with water and was collected by filtration and recrystallized from methanol to give 0.168 g (71% yield) of white needles. Mp: 180 °C. IR(KBr) ν_{max} cm^{-1}: 3304(br,NH), 2220(CN), 2182(CN), 1560, 1456, 1336, 1244. ^{1}H-NMR($CDCl_3$)δ: 9.30(1H,brs,NH), 7.67(1H,d,J = 3.0Hz,7-H), 7.24-7.46(1H,m,4,5,6-H), 3.49(3H,brs,N-Me), 3.06(3H,brs,N-Me). UV(ethanol)λ_{max} nm(log ε): 255(3.93), 277(4.07), 303(4.19), 326(4.17).

5.19. 2-Cyano-3-(3-indolyl)-3-morpholino acrylonitrile (10c)

This compound was obtained from 0.218 g of **10a** mixed with excessive amount of morpholine in a similar manner to that of **10b**, giving 0.267 g (96% yield) of white needles. Mp:198–199. IR(KBr) ν_{max} cm^{-1}: 3649(NH), 2207(CN), 2199(CN), 1517, 1446, 1112, 753. ^{1}H-NMR($CDCl_3$)δ: 9.19(1H,s,N−H), 7.73(1H,d,J = 3.3 Hz,2-H), 7.42–7.51(2H,m,aromatic-H), 7.27–7.34 (2H,m,aromatic-H), 3.88(8H,w,N−CH2−CH_2−O). UV(ethanol) λ_{max} nm(log ε): 256(3.67), 276(3.73), 312(3.96).

5.20. 2,3-Dicyano-3-(1-methyl-2-phenyl)indol-1-yl-acrylonitrile (11a)

This compound was synthesized via the scheme in reference [8]. Mp:208–209 °C. IR(KBr) ν_{max} cm^{-1}: 2217(CN), 1515, 1471, 1394, 1083, 767, 750. ^{1}H-NMR($CDCl_3$)δ: 7.40–7.79(10H,m,NH,4,5,6,7-H,ph-H), 3.79(3H,S,NMe). UV(ethanol)λ_{max} nm(log ε): 286(4.30), 468(4.18).

5.21. 2-Cyano-3-(1-methyl-2-phenyl)indol-3-yl-3-dimethylamino acrylonitrile (11b)

This compound was obtained from 0.308 g of **11a** mixed with excessive amount of dimethylamine in a similar manner to that of **10b**, giving 0.302 g (93% yield) of white needles. Mp:178–179 °C. IR(KBr) ν_{max} cm^{-1}: 2930, 2204(CN), 2195(CN), 1550, 1407, 748. ^{1}H-NMR($CDCl_3$)δ: 2.78(3H,S,N-Me), 3.31(3H,S,N-Me), 3.75(3H,S,N-Me), 7.28–7.51(9H,m,4,5,6,7-H,ph-H). UV(ethanol)λ_{max} nm(log ε): 289(4.12).

5.22. 2-Cyano-3-(1-methyl-2-phenyl)indol-3-yl-3-morpholino acrylonitrile (11c)

This compound was obtained from 0.161 g of **11a** mixed with excessive amount of morpholine in a similar manner to that of **10b**, giving 0.678 g (92% yield) of white needles. Mp:227–228 °C. IR(KBr) ν_{max} cm^{-1}: 2958, 2860, 2207(CN), 2189(CN), 1513, 1486, 1113, 742. ^{1}H-NMR($CDCl_3$)δ: 7.54–7.66(4H,m,animotic-H), 7.31–7.46(5H,m,animotic-H), 3.76(3H,S,NMe), 2.95–4.00(8H,m,N−CH2−CH_2−O). UV(ethanol)λ_{max} nm(log ε): 290 (4.32).

5.23. 2,3-Dicyano-3-(1-methyl)indol-3-yl-acrylonitrile (12a)

This compound was synthesized via the scheme in reference [8]. Mp:220–221 °C. IR(KBr) ν_{max} cm^{-1}: 3131, 2212(CN), 1509, 1469, 1401, 1241, 756. ^{1}H-NMR($CDCl_3$)δ: 3.98(3H,S,N-Me), 7.43–7.48 (1H,m,7-H), 8.34–8.40(3H,m,4,5,6-H), 8.54(1H,S,2-H). UV(ethanol) λ_{max} nm(log ε): 252(3.91), 287(3.96), 462(4.38).

5.24. 2-Cyano-3-(1-methyl)indol-3-yl-3-dimethylamino acrylonitrile (12b)

This compound was obtained from 0.348 g of **12a** mixed with excessive amount of dimethylamine in a similar manner to that of **10b**, giving 0.268 g (71% yield) of white needles. Mp:148–149 °C. IR(KBr) ν_{max} cm^{-1}: 3449, 2935, 2203(CN), 2190(CN), 1536, 1408, 1246, 748. ^{1}H-NMR($CDCl_3$)δ: 3.26(6H,gr,N-Me2), 3.89(3H,S,N-Me), 7.29–7.43(9H,m,4,5,6,7-H,ph-H), 7.63(1H,S,2-H). UV(ethanol) λ_{max} nm(log ε): 282(4.07), 305(4.20), 326(4.18).

5.25. 2-Cyano-3-(1-methyl)indol-3-yl-3-morpholino acrylonitrile (12c)

This compound was obtained from 0.308 g of **12a** mixed with excessive amount of morpholine in a similar manner to that of **10b**, giving 0.213 g (73% yield) of white needles. Mp:185 °C. IR(KBr) ν_{max} cm^{-1}: 3466, 3112, 2206(CN), 1537, 1473, 1439, 1117,749. ^{1}H-NMR($CDCl_3$)δ: 7.67(1H,S,2-H), 7.28–7.49(4H,m,4,5,6,7-H), 3.94(3H,S,N-Me), 3.60–4.10(8H,m,N–CH2–CH_2–O). UV(ethanol)λ_{max} nm(log ε): 262(4.10), 279(4.11), 312(4.35).

References

[1] Padwa A, editor. 1,3-dipolar cycloaddition chemistry. New York: John Wiley & Sons; 1984.

[2] Mizuyama N, Tominaga Y, Kohra S, Ueda K, Hirayama S, Shigemitsu Y. Synthesis and steady-state spectroscopic study of 5-aryl-2,2′-bipyridyls. New fluorescent compounds in solid state. Bull Chem Soc Jpn 2006;79:602–11.

[3] Mizuyama N, Murakami Y, Kohra S, Ueda K, Hiraoka K, Nagaoka J, et al. Synthesis and fluorescence of 2H-pyrone derivatives for organic light-emitting diodes (OLED). J Heterocyclic Chem 2007;44:115–32.

[4] Yuan Z, Collings JC, Taylor NJ, Marder TB, Jardin C, Halet J-F. Linear and nonlinear optical properties of three-coordinate organoboron compounds. J Solid State Chem 2000;154:5–12.

[5] Fujikawa Y, Urano Y, Komatsu T, Hanaoka H, Kojima H, Terai T, et al. Design and synthesis of highly sensitive fluorogenic substrates for glutathione S-transferase and application for activity imaging in living cells. J Am Chem Soc 2008;130:14533–43.

[6] Shinar J, editor. Organic light-emitting devices. New York: Springer-Verlag; 2004.

[7] Sun M, Pullerits T, Kjellberg P, Beenken WJD, Han K. Control of emission by intermolecular fluorescence resonance energy transfer and intermolecular charge transfer. J Phys Chem A 2006;110:6324–8.

[8] Ruthmann J, Kovalenko SA, Ernsting NP, Ouw DJ. Femtosecond relaxation of 2-amino-7-nitrofluorene in acetonitrile: observation of the oscillatory contribution to the solvent response. J Chem Phys 1998;109:5466–8.

[9] Petsalakis ID, Georgladou DG, Vasilopoulou M, Pistolis G, Dimotikali D, Argtis P, et al. Theoretical investigation on the effect of protonation on the absorption and emission spectra of two amine-group-bearing, red "push–pull" emitters, 4-dimethylamino-4′-nitrosostilbene and 4-(dicyanomethylene)-2-methyl-6-*p*-(dimethylamino)-4*H*-Pyran, by DFT and TDDFT calculations. J Phys Chem A 2010;114:5580–7.

[10] Marques MAL, Ullrich CA, Nogueira F, Rubio A, Burke K, Gross EKU, editors. Time-dependent density functional theory, vol. 706. Heidelberg: Springer-Verlag; 2006. Lecture Note in Physics.

[11] Deligeorgiev T, Lesev N, Kaloyanova S. An improved method for tricyanovinilation of aromatic amines under ultrasound irradiation. Dyes Pigm 2011;91:74–8.

[12] Sausen GN, Engelhardt VA, Middleton WJ. Cyanocarbon chemistry. VII.1 Tricyanoethylenes. J Am Chem Soc 1958;80:2815–22.

[13] El-Nahass MM, Abd-El-Rahman KF, Darwish AAA. Electrical conductivity of 4-tricyanovinyl-N, N-diethylaniline. Physica B Condensed Matter 2008;403:219–23.

[14] McCormac T, Farrell D. Electrochemical investigation into the interaction between various pyrrole moieties and the well-known electron acceptor, tetracyanoethylene. Electrochim Acta 2001;46:3287–99.

[15] Tawada Y, Tsuneda T, Yanagisawa S, Yanai T, Hirao K. A long-range-corrected time-dependent density functional theory. J Chem Phys 2004;120:8425–33.

[16] Yanai T, Tew DP, Handy NC. A new hybrid exchange-correlation functional using the Coulomb-attenuating method (CAM-B3LYP). Chem Phys Lett 2004;393:51–7.

[17] Cossi M, Scalmani G, Rega N, Barone V. New developments in the Polarizable Continuum Model for quantum mechanical and classical calculations on molecules in solution. J Chem Phys 2002;117:43–55.

[18] Shigemitsu Y, Komiya K, Mizuyama N, Tominaga Y. TD-DFT investigation on the electronic spectra of novel N-methylmaleimides linked with indolizine ring system. J Mol Struct (THEOCHEM) 2008;855:92–101.

[19] Gaussian 09. Wallingford CT: Gaussian, Inc.; 2009.

[20] Karlström G, Lindh R, Malmqvist P-Å, Roos BO, Ryde U, Veryazov V, et al. MOLCAS ver.7.4. Comp Mater Sci 2003;28:222–39.

[21] Nishimoto K. A MO theoretical study of organic dyes I. Effect of chemical softness on the electronic spectra. Bull Chem Soc Jpn 1993;66:1876–80.

[22] Furche F, Burke K, Spellmeyer DC, editors. Annual reports in computational chemistry, vol. 1. Elsevier; 2005. p. 19–30.

[23] Jacquemin D, Perpète EA, Scalmani G, Frisch MJ, Kobayashi R, Adamo C. Assessment of the efficiency of long-range corrected functionals for some properties of large compounds. J Chem Phys 2007;126:144105.

[24] Mennucci B, Cappelli C, Guido CA, Cammi R, Tomasi J. Structures and properties of electronically excited chromophores in solution from the Polarizable Continuum Model coupled to the time-dependent density functional theory. J Phys Chem A 2009;113:3009–20.

[25] Amatatsu Y. Skeletal relaxation effect on the charge transfer state formation of 4-dimethylamino,4′-cyanostilbene. J Phys Chem A 2006;110:8736–43.

[26] Swalina C, Maroncelli M. Nonradiative deactivation in benzylidene malononitriles. J Phys Chem C 2010;114:5602–10.

[27] Clarke TM, Gordon KC, Kwok WM, Phillips DL, Officer DL. Tuning from π,π^* to charge-transfer excited states in styryl-substituted terthiophenes: an ultrafast and steady-state emission study. J Phys Chem A 2006;110:7696–702.

[28] Improta R, Scalmani G, Frisch MJ, Barone V. Toward effective and reliable fluorescence energies in solution by a new state specific Polarizable Continuum Model time dependent density functional theory approach. J Chem Phys 2007;127:074504–13.